Three-Dimensional Submodeling of Stress Concentrations

J. R. Beisheim
ANSYS, Inc., Canonsburg, PA 15317
G. B. Sinclair
Department of Mechanical Engineering
Louisiana State University, Baton Rouge, LA 70803

Abstract

Stress concentrations are a concern in engineering because of their implications regarding structural integrity. Efficiently and accurately computing the associated stresses is therefore important. Unfortunately it is not always an easy task. This task becomes more challenging when the complex configurations encountered in practice require three-dimensional analysis. Submodeling with finite element analysis is one means available to meet this challenge. With submodeling, a subregion is broken out from the original global region and analyzed separately. This subregion requires boundary conditions taken from the finite element analysis of the global region. Accurately estimating the errors associated with these boundary conditions is critical to controlling them and thereby enabling efficient submodeling. In this paper, we outline a two-dimensional submodeling procedure that addresses this issue, then show how it can be extended for three-dimensional analyses. We check the procedure on a three-dimensional test problem with a known exact solution. The analysis of this problem illustrates the improved stress results that one can get with the submodeling procedure in return for moderate computational effort.

Introduction

Background and Motivation

The stresses attending stress concentrations are often a major contributor to the failure of components. It follows that the accurate evaluation of these stresses is of importance in engineering. To be reasonably certain that such stresses are indeed sufficiently accurately computed when using finite element analysis (FEA) requires convergence checks. In real engineering applications, this typically requires a sequence of at least three successively refined grids. Further, successive grids in this sequence should represent significant refinement over predecessors. One means of realizing significant refinement is by forming successive grids by halving elements sides. In two-dimensions, this leads to quadrupling of the numbers of elements and thus a third grid with 16 times as many elements as the originating grid. This third grid can consequently tax computational facilities. In three-dimensions, this situation is considerably more taxing. This is because halving element sides increases element numbers by a factor of eight, and hence a third grid with 64 times as many elements as the original. Moreover, 3-D elements entail more degrees of freedom per element than 2-D, usually more elements are required with the initial grid, and the ultimate stress concentration in 3-D can be markedly higher than in 2-D. Accordingly, it is not hard to exhaust computational capabilities when attempting to obtain converged and accurate peak stresses with three-dimensional FEA. One means of reducing this computational burden is *submodeling*.

Submodeling Overview

Submodeling involves running an initial global analysis that includes the local region with the stress concentration of interest. A subregion, or submodel, around this region of interest is broken out and analyzed separately. An example is illustrated in Figure 1. Figure 1(a) shows the initial global finite

element grid and Figure 1(b) is a close-up of the contact region. At the edge of contact, where the peak stress occurs, the small darkened areas represent the submodel region (these areas have had grid lines around them removed to distinguish them better). Figure 1(c) shows the coarse grid for this submodel region. "Boundary" conditions taken from the FEA with the initial global grid are then applied to the refined submodel grids. In the example of Figure 1, these quantities are applied on the boundaries AB, BC, CD, and their primed counterparts. Generally, these FEA boundary conditions have not converged to the exact boundary conditions, and therefore have some error associated with them. This *boundary condition error* must be controlled to realize accurate converged results when using submodeling.

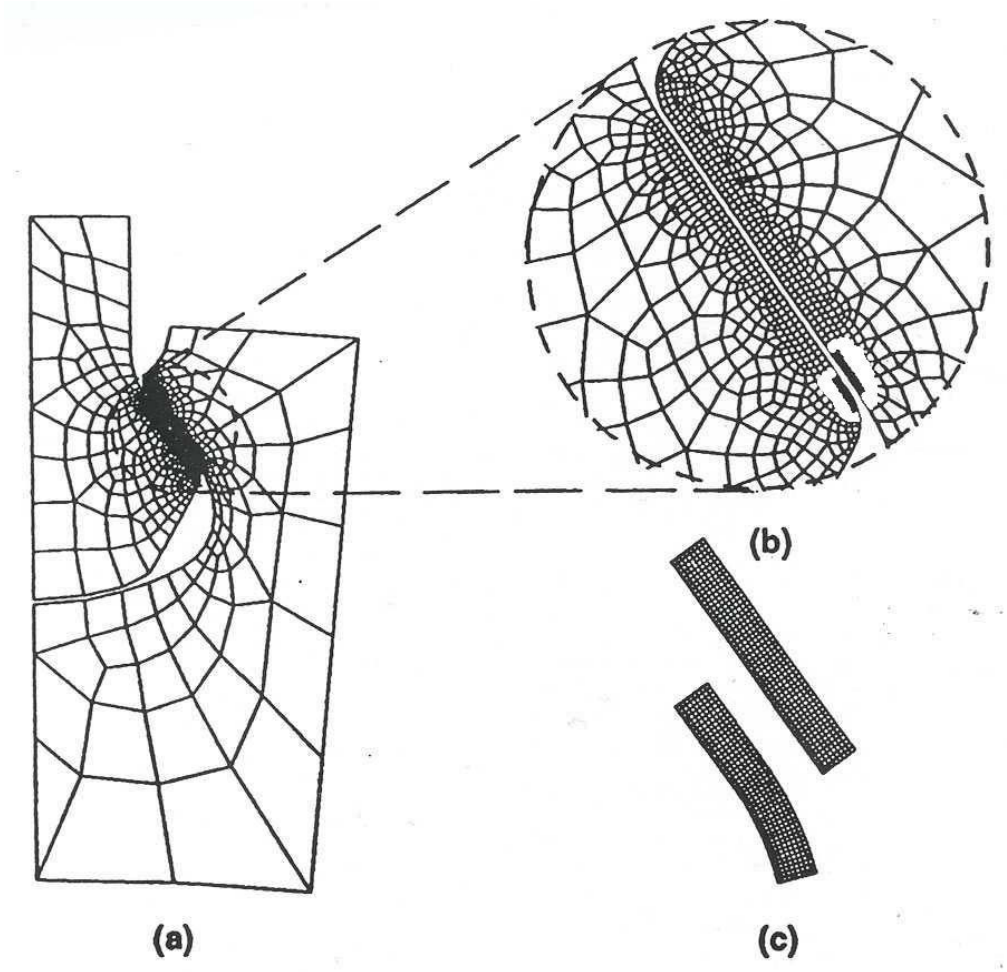

Figure 1 - Dovetail blade attachment for a gas turbine engine: (a) global grid, (b) close-up of contact region in global grid, (c) submodel grid

Literature Review

Submodeling is referred to in the literature by a variety of other terms (e.g., zooming, global-local analysis, windowing, rezoning, and substructuring), and a number of approaches to submodeling exist in the literature. A recent survey of these various approaches is given in Cormier *et al*. (Reference 1). Predominantly these approaches are concerned with two-dimensional analysis. Some of these approaches are applied to three-dimensional applications: Ransom and Knight (Reference 2), Whitcomb and Woo (References 3,4), and Srinivasan *et al*. (Reference 5). However, none of these approaches are applied to true test problems in three-dimensions. Here by true test problems we mean problems with known exact solutions which thereby avoid any ambiguity whatsoever as to the errors incurred in their analysis. Consequently it is not completely clear how well any of the three-dimensional submodeling approaches

reported in the literature control boundary condition error, and thus realize converged and accurate peak stresses.

Present Submodeling Procedure

Here we seek to provide a procedure for obtaining converged results for three-dimensional elastic stresses. The particular procedure adopted extends the submodeling approach given in Cormier *et al*. (Reference 1) and Sinclair *et al*. (Reference 6). We choose to follow References 1 and 6 because they would appear to offer the greatest computational efficiency by having the largest reduction in the size of the submodel region relative to the size of the global region. Specifically, the ratio of the global area to that of the submodel of the procedure found in References 1 and 6 is typically forty times greater than the other procedures found in the literature, resulting in greater computational savings. We offer some improvements to this procedure and adapt it to three-dimensions. We then apply the resulting submodeling procedure to a three-dimensional contact problem with a known exact solution.

Outline of Remainder of Paper

In what follows, in the next section we outline our submodeling procedure for two-dimensional finite element analysis. Also in the next section, we provide some justification for our estimates of the two error sources that accompany submodeling and an improved means of estimating one of these error sources, the discretization error. We then describe how the procedure is extended to three-dimensional analysis (details of the bicubic surface required are provided in Appendix 1). Then, in the following section, we demonstrate our submodeling procedure on a three-dimensional test problem involving contact between a rigid, right-circular cylinder and an elastic half-space (some details of this test problem are furnished in Appendix 2).

Submodeling Procedure

Global Three-dimensional Analysis

To check for convergence, we begin with a global analysis that is run using three systematically-refined grids which we label coarse, medium, and fine. As suggested in the Introduction, elements in successive grids are in fact formed by halving, or at least nearly halving, element sides.[1] As also noted in the Introduction, this approach to grid refinement in three-dimensional FEA can easily lead to a fine grid that is not computationally tractable. To avoid this we proceed as follows. We first estimate the maximum number of degrees of freedom that the available computational facilities can handle. Then we design a fine grid with about this number of degrees of freedom or somewhat fewer. Thereafter we successively coarsen this grid by combining sets of typically eight elements to furnish a medium grid then a coarse grid. In this way we arrive at a computationally tractable set of global grids on which convergence can be checked.

Upon running the three global grids, we apply convergence checks to the desired peak stress component. The first such convergence check determines whether the peak stress is *converging*. The peak stress is judged converging if

$$\left|\sigma^{m}_{\max} - \sigma^{c}_{\max}\right| > \left|\sigma^{f}_{\max} - \sigma^{m}_{\max}\right| \tag{1}$$

where the superscripts identify the coarse, medium, and fine global grids on which the peak stress, $\sigma_{\max}$, is calculated. The second convergence check determines whether the peak stress is *converged*. The peak stress is judged converged if

[1] Some justification for this approach to convergence checks in stress analysis with FEA is given in Sinclair (Reference 7).

$$\left| \frac{\sigma^{f}_{\max} - \sigma^{m}_{\max}}{\sigma^{f}_{\max}} \right| < \varepsilon_s \tag{2}$$

where ε_s is the error level sought in the analysis. For peak stress results, we view an $\varepsilon_s = 0.01$ as leading to excellent accuracy, $\varepsilon_s = 0.05$ as good, and $\varepsilon_s = 0.10$ as satisfactory. Of course, if the peak stress is judged to be converging and to have converged to within ε_s, the analysis is complete. Otherwise we proceed with the submodeling procedure.

Two-dimensional Submodeling

Here we first explain the submodeling procedure as used in two-dimensional analysis. This procedure largely follows that of Cormier *et al*. (Reference 1). We modify the procedure in Cormier *et al*. (Reference 1) somewhat by offering an improved means of reliably estimating the two error sources that accompany submodeling.

The first step of the submodeling procedure in two-dimensions is locating the boundaries of the submodel region and, as a result, establishing the size of the submodel region. Clearly the maximum sought-after stress component has not converged otherwise there would be no need to submodel. Away from this maximum stress location, however, it can converge. We choose distances away from the peak stress location and check that the sought-after stress component is converging in accordance with (1), and has converged as in (2). The positions closest to the maximum stress location where the sought-after stress component has converged set the extents of the submodel region.

Next, we discretize the submodel region with its own coarse, medium, and fine grids. Typically these grids are uniform, thereby enabling completely systematic refinement. The size of the elements in the coarsest of these grids corresponds to that of the next grid in the global sequence if one were to continue to refine this sequence, and hence is smaller than the fine global grid. These submodel grids require conditions on parts of their boundaries to be taken from the global FEA. We choose to use displacements in these conditions in what follows.

After selecting and discretizing the submodel region, we check for converging displacements from the global FEA along those parts of the boundaries of the submodel interior to the global region. That is, in the example of Figure 1, on the boundaries AB, BC, CD, and their primed counterparts. Knowing that the sought-after stress is converging at this distance away from the peak stress location and that displacements converge more rapidly than stresses,[2] it is likely that the displacements are also converging. Indeed, this more rapid convergence is the reason for choosing displacements over stresses as boundary conditions in our submodel.[3] Analogous to (1), the boundary displacements are judged *converging* if

$$\left| u_i^{c} - u_i^{m} \right| > \left| u_i^{m} - u_i^{f} \right| \tag{3}$$

at practically every boundary node. In (3), u_i represent the displacements at a given node and the superscripts continue to identify the particular grid used in their evaluation. Given the boundary displacements are judged to be converging, we continue with the submodeling procedure.

Next, we fit cubic splines to the converging nodal displacements. The interpolation of these displacements is necessary to obtain intervening values between the nodes of the global fine grid even for the coarsest of submodel grids. Cubic splines are used because they are continuous and continuously differentiable, as are the displacements they are trying to replicate. Further, they avoid the introduction of spurious log singularities in boundary stresses that typically accompanies the use of displacement shape functions for interpolation (see Sinclair and Epps, Reference 9).

Using the fitted boundary displacements, we run our three submodel grids and check whether the applied submodel boundary conditions have *converged*. To determine if the displacements in the boundary

---

[2] See, e.g., Strang and Fix (Reference 8).

[3] Some numerical evidence of the superiority of displacements over stresses in submodel boundary conditions is given in Sinclair *et al*. (Reference 6).

conditions are converged we must recognize and separate the two sources of error that accompany submodeling. The first source of error is *boundary condition error*. We define ε_{bc} as our estimate of this source of error by

$$\varepsilon_{bc} = \frac{\sigma_{\max}^{fbc} - \sigma_{\max}^{mbc}}{\sigma_{\max}^{fbc}} \tag{4}$$

where $\sigma_{\max}^{fbc}$ and $\sigma_{\max}^{mbc}$ are evaluated on the fine submodel grid using boundary conditions taken from the fine global grid and medium global grid respectively. The other source of error is the *discretization error* that is inherent with FEA. We define ε_d as our estimate of this source of error by

$$\varepsilon_d = \frac{\sigma_{\max}^{fs} - \sigma_{\max}^{ms}}{\sigma_{\max}^{fs}} \tag{5}$$

where $\sigma_{\max}^{fs}$ and $\sigma_{\max}^{ms}$ are evaluated on the fine submodel grid and medium submodel grid, respectively, using boundary conditions taken from the fine global grid. With these definitions, our estimate of the total error, ε, results from simply adding both the boundary condition error and discretization error. That is

$$\varepsilon = \varepsilon_{bc} + \varepsilon_d \tag{6}$$

With this means, two different situations arise: One when ε_{bc} and ε_d are of opposite signs and cancel each other to a degree, the other when they are of the same sign and accumulate. To ensure the magnitude of the actual total error is less than the error level sought in our analysis we therefore take:

$$\begin{gathered} |\varepsilon_{bc}| < \varepsilon_s \quad \text{and} \quad |\varepsilon_d| < \varepsilon_s \quad \text{if} \quad \varepsilon_{bc}\varepsilon_d < 0 \\ |\varepsilon_{bc}| < \alpha\varepsilon_s \quad \text{and} \quad |\varepsilon_d| < (1-\alpha)\varepsilon_s \quad \text{if} \quad \varepsilon_{bc}\varepsilon_d > 0 \end{gathered} \tag{7}$$

In the second of (7), α is a number between 0 and 1. Consequently the second of (7) is a more stringent criterion than the first. The key difference between our procedure and the procedure found in Cormier *et al*. (Reference 1) involves separating the two error sources that accompany submodeling and thus recognizing when these two error sources accumulate. By separating and calculating both sources of error, our procedure is able to more reliably achieve accurate converged results.

Justification of Error Estimates

Here we provide some justification for our means of estimating the two sources of error that accompany submodeling. The fine submodel grid with the best available boundary conditions represents our best estimate of the exact peak stress. For this estimate, the actual total error, ε_a, is

$$\varepsilon_a = \frac{\sigma_{\max}^{e} - \sigma_{\max}^{fs}}{\sigma_{\max}^{e}} \tag{8}$$

where $\sigma_{\max}^{fs}$ is found on the fine submodel grid with the boundary conditions from the fine global grid, and $\sigma_{\max}^{e}$ is the exact solution. Then two contributions to ε_a can be distinguished. These are the actual submodel boundary condition error, ε_{bc}^a, and the actual submodel discretization error, ε_d^a. Thus

$$\varepsilon_a = \varepsilon_{bc}^a + \varepsilon_d^a \tag{9}$$

Introducing expressions for these actual errors then gives

$$\varepsilon_a = \left.\frac{\sigma_{\max}^{ebc} - \sigma_{\max}^{fbc}}{\sigma_{\max}^{e}}\right|_{fs} + \left.\frac{\sigma_{\max}^{e} - \sigma_{\max}^{ebc}}{\sigma_{\max}^{e}}\right|_{fs} \tag{10}$$

Here, as indicated by the subscripted bars, all finite element results are obtained on the fine submodel grid, and $\sigma_{\max}^{ebc}$ is such a finite element result evaluated using exact boundary conditions. Since $\left.\sigma_{\max}^{fbc}\right|_{fs}$ equals $\sigma_{\max}^{fs}$ in (8), combining the two terms in (10) recovers (8). Observe, though, that this is only true when ε_{bc}^{a} and ε_{d}^{a} are assigned signs in accordance with (10).

It follows from (9) and (10) that we need to estimate each contribution to the actual total error because in an actual application we will not have available $\sigma_{\max}^{e}$ or $\sigma_{\max}^{ebc}$. Then (4), evaluated on the fine submodel grid, represents the best available estimate of ε_{bc}^{a}, while (5) represents the best available simple estimate of ε_{d}^{a}. Hence the adoption of (4), (5), and (6) as our means of estimating the actual total error.

Improved Estimate of Discretization Error

It is possible to improve error estimation further in submodeling by adopting a superior estimate of the discretization error, ε_d. When grid refinement entails successively halving element sides, the estimate in (5) typically overestimates discretization error. For linear convergence, (5) is an accurate estimate. However, for quadratic convergence (5) overestimates by a factor of three, for cubic convergence by a factor of seven, and so on. To obtain better estimates when convergence is faster than linear, we proceed as follows. From (8), (9)

$$\sigma_{\max}^{e} - \sigma_{\max}^{fs} = \sigma_{\max}^{e}\varepsilon_{bc}^{a} + \sigma_{\max}^{e}\varepsilon_{d}^{a} \tag{11}$$

where, as in (8), $\sigma_{\max}^{fs}$ is evaluated with boundary conditions from the fine global grid. Now model the discretization error with

$$\varepsilon_{d}^{a} = Ch^{\lambda} \tag{12}$$

wherein h is the mesh size, C a constant, and λ the convergence rate ($\lambda = 1$ for linear, $\lambda = 2$ for quadratic, etc.,). Introducing (12) into (11) and rearranging gives

$$\hat{\sigma} - \sigma_{\max}^{fs} = Ch^{\lambda}\sigma_{\max}^{e} \tag{13}$$

where $\hat{\sigma} = \sigma_{\max}^{e}(1 - \varepsilon_{bc}^{a})$. Now ε_{bc}^{a} can be expected to be the same for the other submodel grids. Hence applying (13) to these grids, when successive grids are formed by halving element sides, gives

$$\begin{aligned} \hat{\sigma} - \sigma_{\max}^{ms} &= C(2h)^{\lambda}\sigma_{\max}^{e} \\ \hat{\sigma} - \sigma_{\max}^{cs} &= C(4h)^{\lambda}\sigma_{\max}^{e} \end{aligned} \tag{14}$$

where calculated $\sigma_{\max}$ continue to be with boundary conditions from the fine global grid. Solving (13), (14) for $\hat{\sigma}$ by dividing (13) by the first of (14) then dividing the first of (14) by the second and equating results, gives

$$\hat{\sigma} = \frac{(\sigma_{\max}^{ms})^2 - \sigma_{\max}^{fs}\sigma_{\max}^{cs}}{2\sigma_{\max}^{ms} - \sigma_{\max}^{fs} - \sigma_{\max}^{cs}} \tag{15}$$

With $\hat{\sigma}$ determined via (15), we can obtain an improved estimate of discretization error from (12), (13) on replacing $\sigma_{\max}^{e}$ with $\sigma_{\max}^{fs}$. Thus

$$\varepsilon_d = \frac{\hat{\sigma} - \sigma_{\max}^{fs}}{\sigma_{\max}^{fs}} \tag{16}$$

This estimate coincides with our earlier estimate (5) if in fact convergence is linear. If convergence is faster than linear, (15), (16) have the potential of yielding more accurate estimates of discretization error than (5). Note, though, that (15), (16) effectively involve extrapolation to estimate $\hat{\sigma}$. This extrapolation leads to erroneous results if peak stresses are not yet converging on the sequence of submodel grids. Hence it is necessary that peak stresses on submodel grids pass the analogue of (1) if (15), (16) are to be applied.

Three-dimensional Submodeling

Here we explain how to implement the foregoing submodeling procedure for three-dimensional analyses. The key distinctions between using this procedure in three-dimensional FEA rather than two-dimensional FEA involve the sizing of the submodel region and the interpolation of the submodel boundary conditions.

As mentioned in a previous subsection, choosing the submodel boundaries in two-dimensional analysis involves finding the locations where the sought-after stress component has converged. In three-dimensional analysis, these locations can result in a submodel region that is too large. To wit, a submodel region that, with the computational facilities available, does not permit computation on the three grids needed for convergence checks. If this is the case, we in effect revert to the grid refinement approach described for the global region. That is, we size the submodel region so that we can in fact compute results with a discretized grid with elements of the size of the fine submodel grid (element sides 1/8 of the element sides in the fine global grid). Then we coarsen this grid by successively combining sets of eight elements to realize medium and coarse submodel grids. This is a grid sequence that is computationally tractable. Moreover, while the global analysis of the sought-after stress component has not converged at all submodel boundary locations under these circumstances, it is nonetheless quite possible that the global displacements there have converged sufficiently. This is a consequence of the more rapid convergence of displacements over stresses noted earlier.

The interpolation of the submodel boundary conditions in two-dimensions involves fitting displacements on lines. In three-dimensions it involves fitting displacements across surfaces. We choose a bicubic surface because it matches the function, its first derivatives, and its cross derivative at the corner points of each interpolation region. As a consequence it can be shown to result in a surface that is continuous with continuous first derivatives in passing from one interpolation region to the next. Thus our bicubic surface, like the cubic spline, is continuous and continuously differentiable as is any displacement it is trying to replicate.

One form of this bicubic interpolation is given in Appendix 1, and this is the approach used here. Alternatively a code for implementing bicubic interpolation can be found in Press *et al*. (Reference 10).[4] These two methods have been found to give exactly the same results with similar computational effort. Ransom and Knight (Reference 2) provide an alternative smooth interpolation scheme. In essence they fit an elastic plate through each of the respective sets of nodal displacements. This shares with the procedures mentioned above C^1 continuity throughout the submodel boundary surfaces. It does, however, result in large matrix systems as the number of elements increases. The procedure used here has no such matrix system because the individual interpolation regions have closed-form expressions for the constants involved (see Appendix 1). This is thought possibly to offer some computational advantage over the approach of Ransom and Knight (Reference 2).

Irrespective of the means chosen to interpolate, it is important to preserve C^1 continuity throughout submodel boundaries. This is not only because this property is in accord with the elasticity displacements that we are attempting to replicate, but also because the absence of C^1 continuity leads to spurious logarithmic stress singularities on the submodel boundaries. For the three-dimensional case of concern

---

[4] Both of these methods are well suited for the submodel boundary surfaces when eight-node brick elements are used. The use of higher-order elements can result in the need to perform some extra interpolation at the middle of element surface areas (e.g. the twenty-node brick). Consistent with the use of the bicubic surface, the average of one-dimensional cubic spline interpolation in each direction should be used for these additional mid-surface points.

here, the log singularities for in-plane extension (Sinclair and Epps, Reference 9) and anti-plane shear (Sinclair, Reference 11) are both active. This is shown in Aksentian (Reference 12). It is also possible to induce additional log singularities in the corners of surfaces that are peculiar to three-dimensional analyses (this can be shown by an analysis along the lines of Sinclair and Epps, Reference 9).

Test Problem

Problem Formulation

Here we describe a test problem stemming from a periodic array of rigid right-circular cylinders indenting an elastic half-space (Figure 2). We choose the particular test problem described here due to the lack of three-dimensional problems with finite regions containing stress concentrations and having known exact solutions. The periodicity of the chosen test problem allows us to analyze a finite region thereby allowing us to build a finite element model on which we can apply exact quantities as boundary conditions. We provide some details for this problem in Appendix 2. We begin with a formal statement of the problem.

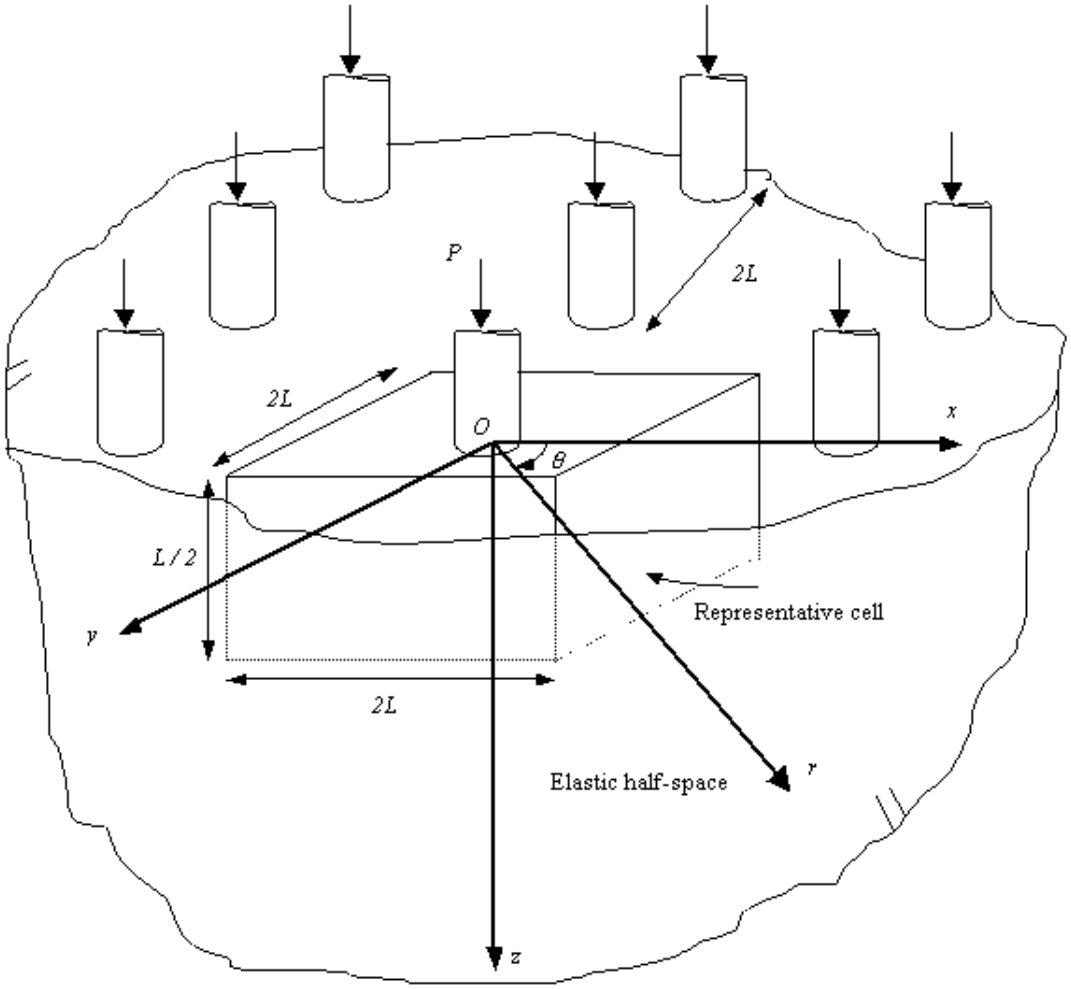

Figure 2 - Array Of Rigid Right-Circular Cylinders Indenting An Elastic Half-Space

The specifics of the geometry chosen for this problem are as follows. The rigid cylinders have a radius a that corresponds to the radius of the contact region. The geometry of the cylinders is most aptly described by cylindrical polar coordinates (r, θ, z). These coordinates share a common origin O with the rectangular Cartesian coordinates (x, y, z) that best describe the half-space. These coordinate systems are related by

$$x = r\cos\theta \qquad y = r\sin\theta \qquad z = z \tag{17}$$

for $0 < r < \infty$, $-\pi < \theta < \pi$, $-\infty < z < \infty$. As mentioned previously, the periodicity of the cylinder array allows us to confine our analysis to a single representative cell that is finite. The symmetry of the geometry and loading allows us to further confine our analysis to a quarter of this cell. We denote this region of the cell as $\Re$. Therefore

$$\Re = \left\{ (x, y, z) \,|\, 0 < x < L,\ 0 < y < L,\ 0 < z < \frac{L}{2} \right\} \tag{18}$$

where $2L$ is the distance between the centers of each cylinder in the periodic array.

The cylinders are not perfect right circular cylinders, so we need to use the following expression to create the bottom surface of the cylinder, w_c,

$$w_c = w_0 \tag{19}$$

at $z = 0$ where w_0 is a function of x and y and is given in Appendix 2. The half-space and cylinder are initially touching with no interpenetration. The rigid cylinder is constrained while tractions are applied to the bottom of the half-space. This causes the half-space, in effect, to displace up into the cylinder and initiate the contact. We these geometric preliminaries in place, we can formally state our test problem as follows.

In general, we seek the stresses σ_x, σ_y, σ_z, τ_{xy}, τ_{xz}, τ_{yz}, and their associated displacements u, v, w, as functions of x, y, and z throughout $\Re$, satisfying: the stress equations of equilibrium in the absence of body forces; the stress-displacement relations for a homogeneous and isotropic, linear elastic solid; the symmetry/periodicity conditions on yz-planes,

$$u = 0 \qquad \tau_{xy} = 0 \qquad \tau_{xz} = 0 \tag{20}$$

on $x = 0, L$ for $0 < y < L$, $0 < z < L / 2$; the symmetry/periodicity conditions on xz-planes,

$$v = 0 \qquad \tau_{xy} = 0 \qquad \tau_{yz} = 0 \tag{21}$$

on $y = 0, L$ for $0 < x < L$, $0 < z < L / 2$; the applied stress conditions on the bottom of $\Re$,

$$\sigma_z = \sigma_0 \qquad \tau_{xz} = \tau_1 \qquad \tau_{yz} = \tau_2 \tag{22}$$

on $z = L / 2$ for $0 < x < L$, $0 < y < L$, where σ_0, τ_1, and τ_2 are expressions given in Appendix 2; the stress-free conditions on the top of the $\Re$ outside the contact region,

$$\sigma_z = 0 \qquad \tau_{xz} = 0 \qquad \tau_{yz} = 0 \tag{23}$$

on $z = 0$ for $0 < x < L$, $0 < y < L$, $a < r$; the frictionless contact conditions,

$$w = w_c \qquad \tau_{xz} = \tau_{yz} = 0 \tag{24}$$

on $z = 0$ for $0 < r < a$, $0 < \theta < \pi / 2$; and finally the inequalities for contact which insist that the contact stress be nowhere tensile inside the contact region and that there be no interpenetration outside.

For this test problem, the peak contact stress is infinite at $r = a$ for $0 \le \theta \le \pi / 2$. Therefore we seek to find an *average* contact stress normal to the contact surfaces of the cylinder and half-space, σ_z at $z = 0$, near the singularity at the edge of contact. The actual average contact stress chosen is an average from $r = 7a/8$ to $r = 2047a/2048$ in increments of $a/128$ along $\theta = 0$. Our last data point is taken slightly away from $r = a$ because the exact contact stress is infinite at $r = a$. We label this average contact stress as $\overline{\sigma}_{\max}$. Its value

is 5.2 times that of the contact stress at the center of the contact region ($r = 0$). This is representative of sort of stress concentrations that occur in practical contact problems (see, e.g., Reference 1). Here we accept a satisfactory answer for $\overline{\sigma}_{\max}$ ($\varepsilon_s = 0.1$) as a reasonable check of our submodeling procedure in three-dimensions because of the additional challenges placed on the approach by having a singular test problem.

As an associated error measure, then, the absolute differences between FEA solutions and the exact solution at each increment in the average are summed and divided by the number of increments and the exact $\overline{\sigma}_{\max}$. By taking absolute differences, we avoid a low error measure that is a result of compensating errors rather than true accuracy.

Finite Element Analysis

Eight-node hexahedral (brick) elements are used to discretize the cylinder and half-space (SOLID45, ANSYS, Reference 13). We use low-order brick elements to facilitate interpolation with the bicubic surface when submodeling. We employ a uniform grid of elements in cylindrical polar coordinates for the cylinder and in rectangular Cartesian coordinates for the half-space. We then systematically refine this grid by halving the element sides. In accordance with the first step of our submodeling procedure, we estimate that the most refined grid our computing resources can accommodate is approximately 150,000 spatial elements. In view of this number, we decide to start with a coarse grid of 256 spatial elements (Figure 3(a)). Systematically refining this grid results in a global medium grid of 2,048 spatial elements, and a global fine grid of 16,384 spatial elements. If both the sought-after average contact stress and the boundary conditions are not converging, then we can still refine our global fine grid and obtain a global superfine grid of 131,072 spatial elements. We do not include the number of spatial elements that represent the rigid cylinder, shown in Figure 3, because in a contact analysis in ANSYS the spatial elements beneath a rigid target surface are not required (the nodes attached to these elements are required). Thus before the solution begins, these elements are deleted to make the solution slightly more efficient.

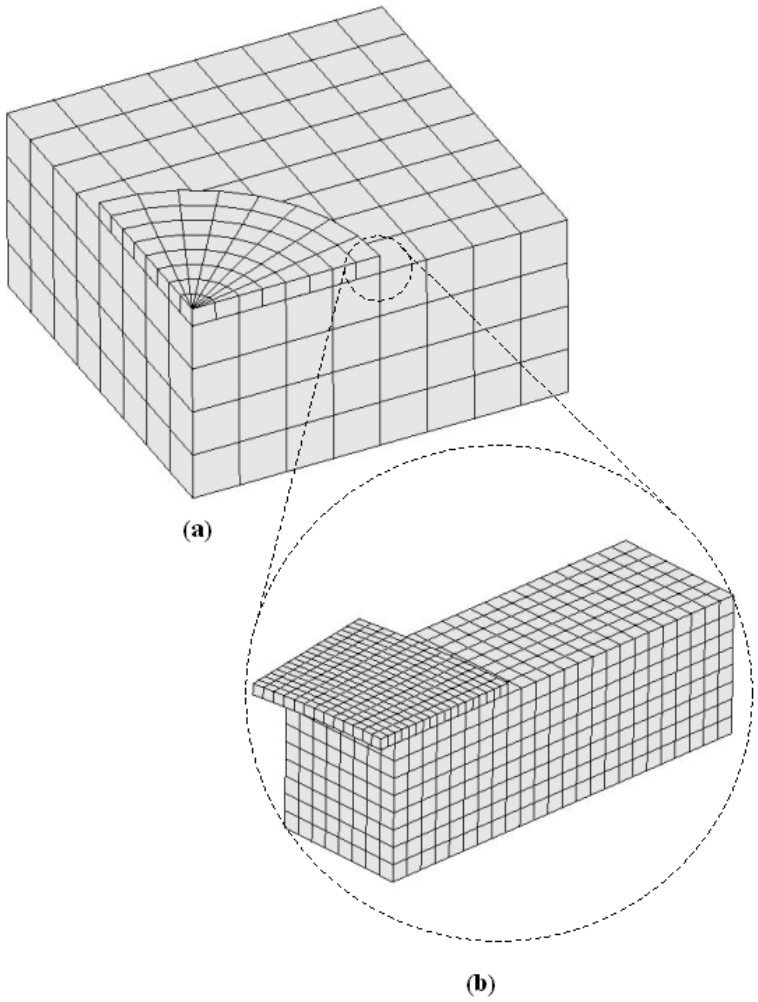

Figure 3 - Finite element grids for test problem: (a) global coarse grid, (b) submodel coarse grid

To police the aforementioned contact conditions between the cylinder and the half-space we use surface-to-surface contact elements (TARGE170 and CONTA173, ANSYS, Reference 13). These contact elements overlay the spatial elements on the contact surfaces at $z = 0$. An important input parameter for these contact elements in ANSYS is the normal contact stiffness factor (FKN). This factor controls the stiffness of the contacting surfaces, which affects the amount of penetration of the contact surface into the target surface. We override the default value of one with a value of 1,000 in order to help limit penetration while still maintaining convergence of the contact algorithm in ANSYS. The total number of spatial and contact elements for each of the global grids is given in Table 1.

Table1 - Number Of Elements In Each Finite Element Grid

FEA Grid	Spatial Elements	Contact Elements	Total Elements
Global Coarse	256	216	472

	Medium	2,048	816	2,864
	Fine	16,384	3,168	19,552
	Superfine	131,072	12,480	143,552
Submodel	Coarse	1,536	722	2,258
	Medium	12,228	2,838	15,126
	Fine	98,304	5,142	103,446

To apply the tractions given in (22) as boundary conditions along the bottom of $\Re$, at $z = L / 2$, we first calculate the value of the traction at the center of each element and multiply this value by one-fourth the area of the element. Then for each node we sum the values from each element that touches that particular node.

Upon running our global coarse, medium, and fine grids we find the sought-after average contact stress, $\overline{\sigma}_{\max}$, is approaching the exact solution. However, we find the average contact stress has not yet converged in accordance with (2). Therefore we decide to use our global superfine grid. With the global superfine grid, $\overline{\sigma}_{\max}$ continues to approach the exact answer but has not converged in the sense of (2). Hence we proceed to submodel.

To begin submodeling, we must first choose the boundaries of the submodel region. We need to choose boundaries far enough in all directions from the location of the peak contact stress to have converged displacement boundary conditions, but close enough to keep the number of degrees of freedom within the limits of our available computational resources. We note here that finding converged boundary conditions for this test problem might be a difficult task given that one boundary of the submodel region must pass through the stress singularity at $r = a$. In this vicinity the FEA displacement solution may not converge. Plotting σ_z from each global grid along lines in three directions from the peak contact stress at $r = a$ and $\theta = 0$ gives us an idea of where the boundary displacements are likely to be converged. We then break out our submodel along uniform grid lines and check that we can obtain three refined grids inside this submodel region that are computationally tractable. As with the global grids, we systematically refine the submodel grids by halving elements. Our submodel coarse grid (Figure 3(b)) then contains element sides that correspond to those found if we had refined the global superfine grid. Thus we have three submodel grids that contain the number of spatial and contact elements shown in the bottom of Table 1. We run our three submodel grids and discuss the results next.

Results

We plot the contact stress, σ_z at $z = 0$, at $\theta = 0$ near $r = a$ for each of our global and submodel grids in Figure 4. Figure 4 illustrates that our results approach the exact solution as we submodel and refine our grids, and that the submodel fine grid most closely matches the exact solution. We can also see in Figure 4 that each FEA grid has a cross-over point where the FEA solution touches the exact solution. This is the result anticipated earlier which leads to compensating errors, and thus the reason absolute values of differences are taken.

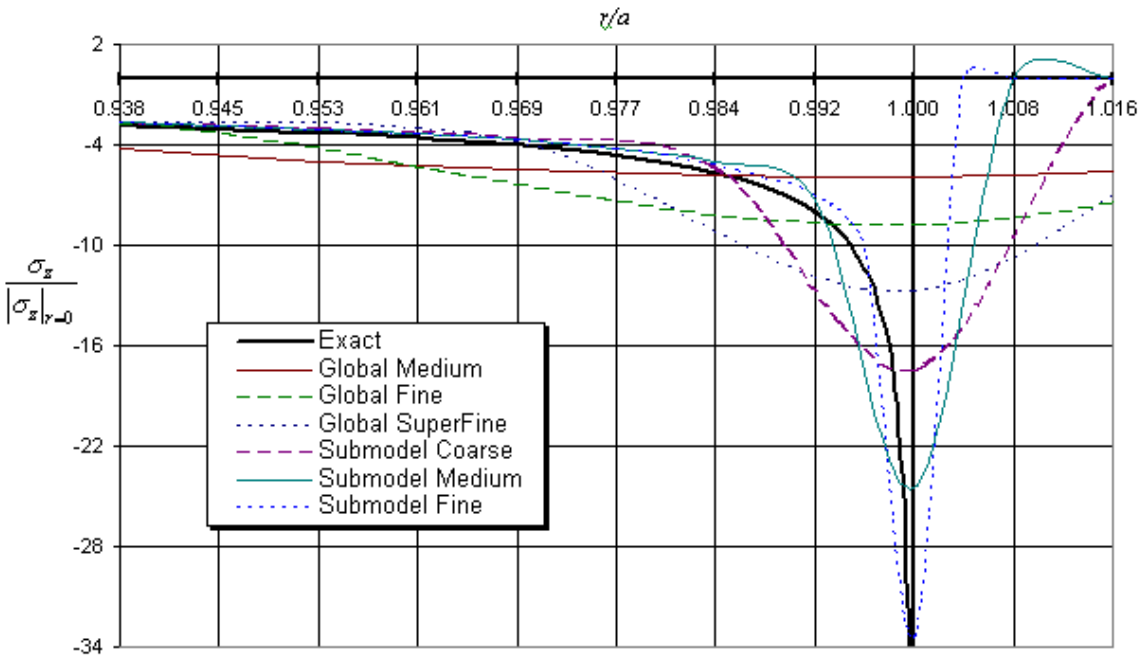

Figure 4 - Plot Of Contact Stresses For Global And Submodel Grids

In completing our submodeling procedure, we must check for convergence in the boundary conditions applied to the submodel. We perform this check by running the sequence of three submodel grids using boundary conditions taken from the global medium grid and comparing these results with those found using boundary conditions taken from the global fine grid. The estimates for the boundary condition error for each submodel grid are given in Table 2. We can see in Table 2 that the boundary condition error can be estimated to be 7.5 percent. We have not run our submodel grids with the exact boundary displacements allowing us to compare our estimate of the boundary condition error with the exact boundary condition error. We plan to proceed with this analysis later. The estimates for the discretization error are also given in Table 2. From there, we can see that the ultimate discretization error can be estimated to be 11.2 percent.

Table 2 - Estimates Of Boundary Condition And Discretization Errors

Grid	ε_{bc} (%)	ε_d (%)
Submodel Coarse	7.4	16.3
Medium	7.5	16.8
Fine	7.5	11.2

Unfortunately, in choosing our error measure in the sought-after average contact stress to entail absolute differences between the FEA solutions and the exact solution, we lose the ability to determine the true signs of the discretization and boundary condition errors. Thus we cannot simply determine whether these errors compensate each other or sum with each other as in the first or second of (7). For this test problem, however, we can obtain the actual errors and hence see if the errors in Table 2 compensate to a degree.

The average contact stress results are also checked for convergence on our sequence of three submodel grids with boundary conditions taken from the global fine grid. We see in Table 3 that differences are decreasing on the submodel grid sequence so that we have convergence in the sense of (1). Note, though,

that (1) is not complied with in the global grid sequence and not complied with between the global and submodel grids. This sort of somewhat erratic convergence is not uncommon in contact problems as the contact extent is located more precisely with each successive grid. This erratic convergence prevents us from using our improved estimate of the discretization error for this problem. Table 3 shows the total actual error to have converged to 6.9 percent. This is satisfactory in itself.

Table 3 - Total Actual Errors

Grid	ε_a (%)	Difference
Global Medium	46.0	
Fine	40.6	4.4
Superfine	33.8	6.8
Submodel Coarse	25.8	
Medium	13.6	12.2
Fine	6.9	6.7

In conclusion, we have demonstrated that by using our submodeling procedure we can achieve accurate and converged contact stresses around the stress singularity for our test problem. Also, our submodeling procedure is more efficient than continuing with global grid refinement (the number of elements in a global grid of comparable refinement to the fine submodel is 67 million).

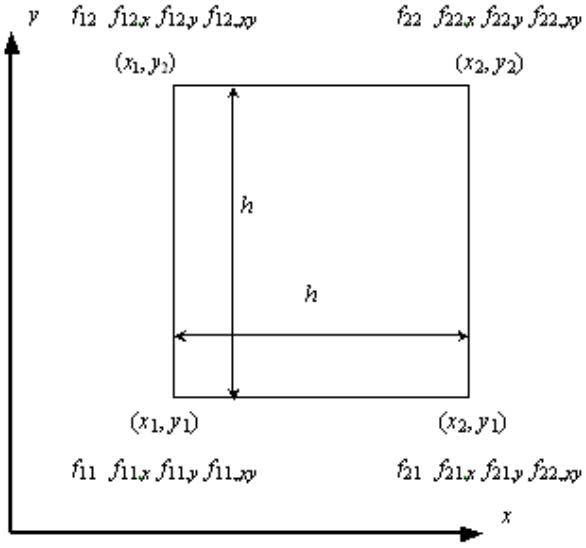

Figure 5 - Representative Region For Interpolation With A Bicubic Surface

Acknowledgements

We are most grateful to General Electric Aircraft Engines Inc. of Cincinnati for providing funding for this research. We are also grateful for ANSYS Inc. of Canonsburg for providing access to their software which is used exclusively throughout.

References

1) N.G. Cormier, B.S. Smallwood, G.B. Sinclair, G. Meda, Aggressive submodelling of stress concentrations. *International Journal for Numerical Methods in Engineering*, 1999, Vol. 46, pp. 889-909.

2) J.B. Ransom, N.F. Knight Jr., Global/local stress analysis of composite panels. *Computers and Structures*, 1990, Vol. 37, pp. 375-395.

3) J.D. Whitcomb, K. Woo, Application of iterative global/local finite element analysis, Part 1: Linear analysis. *Communications in Numerical Methods in Engineering*, 1993, Vol. 9, pp. 745-756.

4) J.D. Whitcomb, K. Woo, Application of iterative global/local finite element analysis, Part 2: Geometrically non-linear analysis. *Communications in Numerical Methods in Engineering*, 1993, Vol. 9, pp. 757-766.

5) S. Srinivasan, S.B. Biggers Jr., R.A. Latour Jr., Identifying global/local interface boundaries using an objective search method. *International Journal for Numerical Methods in Engineering*, 1996, Vol. 58, pp. 805-828.

6) G.B. Sinclair, J.R. Beisheim, B.P. Epps, S.L. Pollice, Towards improved submodeling of stress concentrations. *Proceedings of the Ninth International ANSYS Conference*, 2000, Pittsburgh, Pennsylvania, CD-ROM.

7) G.B. Sinclair, FEA of singular elasticity problems, *Proceedings of the Eighth International ANSYS Conference*, 1998, Pittsburgh, Pennsylvania, Vol. 1, pp. 225-236.

8) W.G. Strang, G.J. Fix, *An Analysis of the Finite Element Method*, Prentice-Hall, Inc., 1973, Englewood Cliffs, New Jersey.

9) G.B. Sinclair, B.P. Epps, On the logarithmic stress singularities induced by the use of displacement shape functions in boundary conditions in submodelling, *Communications in Numerical Methods in Engineering*, 2001, to appear.

10) W.H. Press, S.A. Teukolsky, W.T. Vetterling, B.P. Flannery, *Numerical Recipes in C*, Cambridge University Press, 1992, New York, New York.

11) G.B. Sinclair, Logarithmic stress singularities in two-dimensional and three-dimensional elasticity, *Proceedings of the Twentieth Southeastern Conference of Theoretical and Applied Mechanics*, 2000, Callaway Gardens, Georgia, pp. SM94.1-8.

12) O.K. Askentian, Singularities of the stress-strain state of a plate in the neighborhood of an edge, *Journal of Applied Mathematics*, 1967, Vol. 37, pp. 193-202.

13) ANSYS personnel, *ANSYS Advanced Analysis Techniques*, 1998, Revision 5.5, ANSYS Inc., Canonsburg, Pennsylvania.

14) G.B. Sinclair, Analytical solutions for periodic contact problems, Report SM 1.01, 2001, Dept. Mechanical Engineering, Louisiana State University, Baton Rouge, Louisiana.

Appendix 1

Here we provide details on the bicubic interpolation used to interpolate the displacements on the boundaries of the submodel. The function *f* for interpolating on the square region in Figure 5 is given by

$$
\begin{aligned}
f = {} & \frac{f_{11}}{h^2}(x_2 - x)(y_2 - y) + \frac{f_{21}}{h^2}(x - x_1)(y_2 - y) \\
& + \frac{f_{12}}{h^2}(x_2 - x)(y - y_1) + \frac{f_{22}}{h^2}(x - x_1)(y - y_1) \\
& + c_1(x - x_1)(x_2 - x)^2(y_2 - y) + c_2(x - x_1)^2(x_2 - x)(y_2 - y) \\
& + c_3(x - x_1)(x_2 - x)^2(y - y_1) + c_4(x - x_1)^2(x_2 - x)(y - y_1) \\
& + c_5(x_2 - x)(y - y_1)(y_2 - y)^2 + c_6(x_2 - x)(y - y_1)^2(y_2 - y) \\
& + c_7(x - x_1)(y - y_1)(y_2 - y)^2 + c_8(x - x_1)(y - y_1)^2(y_2 - y) \\
& + c_9(x_2 - x)^2(y_2 - y)^2(x - x_1)(y - y_1) \\
& + c_{10}(x - x_1)^2(y_2 - y)^2(x_2 - x)(y - y_1) \\
& + c_{11}(x_2 - x)^2(y - y_1)^2(x - x_1)(y_2 - y) \\
& + c_{12}(x - x_1)^2(y - y_1)^2(x_2 - x)(y_2 - y) \ .
\end{aligned}
$$

Here

$$
c_1 = \frac{1}{h^3}\left[f_{11,x} + \frac{1}{h}(f_{11} - f_{21}) \right],
$$

$$
c_2 = \frac{-1}{h^3}\left[f_{21,x} + \frac{1}{h}(f_{11} - f_{21}) \right],
$$

$$
c_3 = \frac{1}{h^3}\left[f_{12,x} + \frac{1}{h}(f_{12} - f_{22}) \right],
$$

$$
c_4 = \frac{-1}{h^3}\left[f_{22,x} + \frac{1}{h}(f_{12} - f_{22}) \right],
$$

$$
c_5 = \frac{1}{h^3}\left[f_{11,y} + \frac{1}{h}(f_{11} - f_{12}) \right],
$$

$$
c_6 = \frac{-1}{h^3}\left[f_{12,y} + \frac{1}{h}(f_{11} - f_{12}) \right],
$$

$$
c_7 = \frac{1}{h^3}\left[f_{21,y} + \frac{1}{h}(f_{21} - f_{12}) \right],
$$

$$
c_8 = \frac{-1}{h^3}\left[f_{22,y} + \frac{1}{h}(f_{21} - f_{22}) \right],
$$

$$
c_9 = \frac{1}{h^4}\left[f_{11,,xy} + \frac{1}{h}(f_{11,x} - f_{12,x} - f_{21,x} + f_{11,y}) + \frac{1}{h^2}(f_{11} - f_{12} - f_{21} + f_{22}) \right],
$$

$$
c_{10} = \frac{-1}{h^4}\left[f_{21,,xy} + \frac{1}{h}(f_{21,x} - f_{22,x} + f_{11,y} - f_{21,y}) + \frac{1}{h^2}(f_{11} - f_{12} - f_{21} + f_{22}) \right],
$$

$$
c_{11} = \frac{-1}{h^4}\left[f_{12,,xy} + \frac{1}{h}(-f_{21,x} + f_{11,x} - f_{22,y} + f_{12,y}) + \frac{1}{h^2}(f_{11} - f_{12} - f_{21} + f_{22}) \right],
$$

$$c_{12} = \frac{1}{h^4}\left[f_{22,,xy} + \frac{1}{h}(-f_{22,x} + f_{21,x} + f_{12,y} - f_{22,y}) + \frac{1}{h^2}(f_{11} - f_{12} - f_{21} + f_{22}) \right],$$

and a comma preceding a subscript denotes differentiation with respect to that subscript, e.g., $f_{11,x} = \left.\frac{\partial f}{\partial x}\right|_{x_1,y_1}$.

Appendix 2

Here we provide further details of our test problem. The construction of this test problem is described in Reference 14. The expressions required to complete this problem are given below.

$$w_0 = \frac{P(1-\upsilon)}{2\pi^2 aG}\left[\sum_{n=0} \frac{\sin\frac{n\pi a}{L}}{n^2}\left(\cos\frac{n\pi x}{L} + \cos\frac{n\pi y}{L}\right) + \sum_{n=1}\sum_{m=1} \frac{2\sin\frac{\pi a\sqrt{n^2+m^2}}{L}}{n^2+m^2}\cos\frac{n\pi x}{L}\cos\frac{m\pi y}{L} \right]$$

$$\sigma_0 = \frac{-P}{4L^2} + \frac{-P}{2\pi aL}\left[\sum_{n=0} \frac{\sin\frac{n\pi a}{L}}{n}\left(1+\frac{\pi n}{2}\right)\left(\cos\frac{n\pi x}{L} + \cos\frac{n\pi y}{L}\right)e^{\frac{-\pi n}{2}}\right.$$
$$\left. + \sum_{n=1}\sum_{m=1} \frac{2\sin\frac{\pi a\sqrt{n^2+m^2}}{L}}{\sqrt{n^2+m^2}}\left(1+\frac{\pi}{2}\sqrt{n^2+m^2}\right)\cos\frac{n\pi x}{L}\cos\frac{m\pi y}{L}e^{\frac{-\pi\sqrt{n^2+m^2}}{2}}\right]$$

$$\tau_1 = \frac{-P}{2\pi aL}\left[\sum_{n=0} \frac{\sin\frac{n\pi a}{L}}{n}\left(\frac{\pi n}{2}\right)\left(\sin\frac{n\pi x}{L}\right)e^{\frac{-\pi n}{2}}\right.$$
$$\left. + \sum_{n=1}\sum_{m=1} \frac{2\sin\frac{\pi a\sqrt{n^2+m^2}}{L}}{\sqrt{n^2+m^2}}\left(\frac{\pi n}{2}\right)\sin\frac{n\pi x}{L}\cos\frac{m\pi y}{L}e^{\frac{-\pi\sqrt{n^2+m^2}}{2}}\right]$$

$$\tau_2 = \frac{-P}{2\pi aL}\left[\sum_{n=0} \frac{\sin\frac{n\pi a}{L}}{n}\left(\frac{\pi n}{2}\right)\left(\sin\frac{n\pi y}{L}\right)e^{\frac{-\pi n}{2}}\right.$$
$$\left. + \sum_{n=1}\sum_{m=1} \frac{2\sin\frac{\pi a\sqrt{n^2+m^2}}{L}}{\sqrt{n^2+m^2}}\left(\frac{\pi n}{2}\right)\cos\frac{n\pi x}{L}\sin\frac{m\pi y}{L}e^{\frac{-\pi\sqrt{n^2+m^2}}{2}}\right]$$

where P is the force pushing the cylinder into the half-space, G is the shear modulus, and υ is Poisson's ratio. The exact solution for the resulting contact stress for this problem is

$$\left.\sigma_z\right|_{z=0} = \frac{-P}{2\pi a^2\sqrt{1-(r/a)^2}}$$